AIAA JOURNAL
Vol. 34, No. 3, March 1996

Fictitious Mass Element in Structural Dynamics

Mordechay Karpel* and Daniella Raveh†
Technion—Israel Institute of Technology, Haifa 32000, Israel

Fictitious masses are used to improve the accuracy and efficiency of modal-based structural analyses that involve substructure synthesis, local excitation, and local structural changes. New formulations, which allow easy applications in various subsequent analyses, are given for two categories of fictitious masses: regular and very large. Regular masses are of the order of entire substructures, whereas very large ones are several orders of magnitude larger. The regular fictitious masses are added to selected coordinates of the finite element model for normal-mode analysis, and then removed in a way that produces modes with local deformations near the selected points, in addition to the nominal natural vibration modes. Subsequent analyses of local nature can then be performed in the standard way. Very large masses are used to generate static constraint modes for fixed-boundary modal coupling, and broken modes are used for representing rigid-body relative motion between structural segments with application to loads analysis. The inclusion of fictitious masses as optional elements in standard structural dynamic procedures is facilitated.

Introduction

MANY structural dynamic analyses are performed with the modal approach, which represents the structural displacements by a relatively small set of low-frequency natural vibration modes. These modes, which serve as generalized coordinates, and the associated natural frequencies and generalized masses are extracted from detailed finite element models. The modal approach often reduces the problem size by orders of magnitudes without affecting the important response characteristics significantly. Major inaccuracies may occur, however, when the modal approach is used in cases involving local deformations that are not represented in the considered modes. The use of fictitious masses can provide a solution in these cases.

The fictitious mass (FM) method was first presented by Karpel and Newman[1] in the context of component-mode synthesis, where the natural modes of separate structural components are combined for the natural modes of the combined structure. Earlier works of Hurty[2] and Craig and Bampton[3] based their formulations on the assumption that the motion of each component, as part of the entire structure, is a linear combination of two sets of isolated component modes: 1) a number of low-frequency, fixed-boundary natural vibration modes and 2) all the static constraint modes obtained by imposing a unit displacement on one of the boundary coordinates while holding the remaining boundary coordinates fixed. The resulting model contains the necessary near-boundary structural information, but it might become inefficient when the number of boundary coordinates is large. The model is also somewhat difficult to apply with standard finite element codes because it is based on two different analysis types, static and dynamic, and it needs special treatment when the boundary is statically determined in any direction. When it is statically determined in all directions, Craig and Bampton's method is reduced to the effective mass modeling method of Girard.[4]

A different approach, which requires only one set of modes with free-boundary coordinates, was taken by Goldman[5] and Hou.[6] These methods were more convenient because they used natural vibration modes only. However, with the boundary points unloaded, vital information about the structural deformations near the boundary is not included in the component modes, which leads to inaccuracies and slow convergence with the number of component modes. Benfield and Hruda[7] loaded the free-boundary coordinates with reduced stiffness and mass matrices of the neighboring substructures, and Hintz[8] and Rubin[9] added static attachment modes. These modifications, and those of hybrid coupling methods,[10] improved the free-coordinate results, but they are more difficult to apply, and less efficient in modular, multiconfiguration cases.

The FM coupling method[1] offered a good compromise between the different approaches. A structural component was represented by a single set of free-boundary modes, calculated with the boundary coordinates loaded with relatively large fictitious masses. The added large masses (which were cleaned in the coupling procedure) cause the low-frequency modal information to contain the necessary near-boundary information without adding static constraint modes. A later development of the FM method by Karpel[11] allowed efficient multiconfiguration normal-mode analyses for cases of a central structure connected to several components through statically determined connections. Fictitious masses were used more recently for eigenvalue analysis of control-augmented structures,[12] time-domain flutter analysis with large structural variations,[13,14] and dynamic response to impulsive excitation.[15] FM concepts were also used in modal tests of structural components loaded with added boundary masses.[16–18] The added masses caused the measured data to contain more near-boundary information, which improved subsequent modal coupling and model update processes.

Until now, the FM studies were based on ad hoc formulations that required elaborate deviations from standard finite element procedures. The purpose of the work presented in this paper was to cast the FM method in a new formulation that facilitates easy applications in various subsequent analyses, to clarify some theoretical and physical aspects of using fictitious masses in comparison with other methods, and to explore new aspects of the FM method when very large fictitious masses are used.

Fixed-Boundary Modal Coupling

The equation of motion of a structural component as part of free vibrations of the entire structure can be partitioned as

$$\begin{bmatrix} M_{ii} & M_{ib} \\ M_{ib}^T & M_{bb} \end{bmatrix} \begin{Bmatrix} \ddot{u}_i \\ \ddot{u}_b \end{Bmatrix} + \begin{bmatrix} K_{ii} & K_{ib} \\ K_{ib}^T & K_{bb} \end{bmatrix} \begin{Bmatrix} u_i \\ u_b \end{Bmatrix} = \begin{Bmatrix} 0 \\ F_b \end{Bmatrix} \quad (1)$$

where the displacement vector $\{u\}$ and the mass and stiffness matrices $[M]$ and $[K]$ are partitioned according to the interior (i) and boundary (b) coordinates, and $\{F_b\}$ is the vector of forces applied at the boundary by other components.

We start with the well-known modal coupling method of Craig and Bampton[3] (CB) for subsequent comparison with the FM approach. The fixed-boundary natural modes of the component, $[\phi_n]$, are calculated from the eigenvalue problem associated with the top

Received March 5, 1995; presented as Paper 95-1343 at the AIAA/ASME/ASCE/AHS/ASC 36th Structures, Structural Dynamics, and Materials Conference, New Orleans, LA, April 10–12, 1995; revision received Oct. 10, 1995; accepted for publication Oct. 12, 1995.

*Associate Professor, Faculty of Aerospace Engineering. Member AIAA.
†Graduate Student, Faculty of Aerospace Engineering.

partition of Eq. (1) with $\{u_b\} = 0$. The modes are normalized such that the generalized mass matrix is a unit matrix,

$$[GM_n] \equiv [\phi_n]^T [M_{ii}][\phi_n] = [I] \tag{2}$$

which yields the generalized stiffness matrix

$$[GK_n] \equiv [\phi_n]^T [K_{ii}][\phi_n] = [\omega_n]^2 \tag{3}$$

where $[\omega_n]$ is a diagonal matrix of natural frequencies.

The second group of modes that serve as generalized coordinates are the n_b constraint modes (where n_b is the number of boundary coordinates), $[\phi_c]$, which are defined by the static displacements of the internal coordinates due to successive unit displacements of the boundary coordinates. These modes are calculated from the static equilibrium equation

$$[K_{ii}][\phi_c] + [K_{ib}] = [0] \tag{4}$$

The basic assumption is that the vector of discrete displacements of the component is a linear combination of the normal and constraint modes,

$$\begin{Bmatrix} u_i \\ u_b \end{Bmatrix} = \begin{bmatrix} \phi_n & \phi_c \\ 0 & I \end{bmatrix} \begin{Bmatrix} \xi_n \\ u_b \end{Bmatrix} \tag{5}$$

where $\{\xi_n\}$ is a vector of generalized displacements. The substitution of Eq. (5) in Eq. (1) and premultiplication by the transpose of the transformation matrix yield [considering Eqs. (2–4)]

$$\begin{bmatrix} I & L^T \\ L & M_c \end{bmatrix} \begin{Bmatrix} \ddot{\xi}_n \\ \ddot{u}_b \end{Bmatrix} + \begin{bmatrix} \omega_n^2 & 0 \\ 0 & K_c \end{bmatrix} \begin{Bmatrix} \xi_n \\ u_b \end{Bmatrix} = \begin{Bmatrix} 0 \\ F_b \end{Bmatrix} \tag{6}$$

where the constraint mass matrix is

$$[M_c] = [\phi_c]^T [M_{ii}][\phi_c] + [\phi_c]^T [M_{ib}] + [M_{ib}]^T [\phi_c] + [M_{bb}] \tag{7}$$

which is slightly more general than that of Ref. 3, where $[M_{ib}] = [0]$. The constraint stiffness matrix is

$$[K_c] = [K_{ib}]^T [\phi_c] + [K_{bb}] \tag{8}$$

and the mass-coupling matrix between the constraint and elastic modes is

$$[L] = \left([\phi_c]^T [M_{ii}] + [M_{ib}]^T\right) [\phi_n] \tag{9}$$

The boundary coordinates in Eq. (6) can be superimposed on those of neighboring components for dynamic analysis of the entire structure.

When the boundary is statically determined, the constraint modes $[\phi_c]$ are rigid-body modes, $[K_c]$ is null, and $[M_c]$ becomes the rigid-body mass matrix with respect to the boundary coordinates. A column $\{L\}_k$ of $[L]$ can be used to define the effective mass matrix associated with the kth elastic mode,

$$[M_r]_k = \{L\}_k \{L\}_k^T \tag{10}$$

which can be used to construct effective mass models.[4] It can be shown from Eqs. (2), (7), and (9) that, when all the elastic modes are taken into account (which is not realistic) and when the effects of $[M_{ib}]$ are negligible (which is normally the case), the sum of the effective mass matrices is

$$\sum_{k=1}^{n_n} [M_r]_k \equiv [L][L]^T = [M_c] - [M_{bb}] \tag{11}$$

where the boundary mass matrix $[M_{bb}]$ normally forms a very small portion of the rigid-body mass matrix $[M_c]$. The diagonal values of $[M_r]_k$ can be used as measures for the importance of including the kth mode in the coupled dynamic analysis.

Free Boundary Loaded with Fictitious Masses

The FM method[1,11] is based on natural vibration modes calculated with the boundary coordinates unconstrained but loaded with relatively large fictitious masses $[M_f]$ added to $[M_{bb}]$ in Eq. (1). These modes, $[\bar{\phi}]$, and the associated diagonal matrix of natural frequencies $[\omega_f]$ satisfy

$$\begin{bmatrix} K_{ii} & K_{ib} \\ K_{ib}^T & K_{bb} \end{bmatrix} \begin{bmatrix} \bar{\phi}_i \\ \bar{\phi}_b \end{bmatrix} = \begin{bmatrix} M_{ii} & M_{ib} \\ M_{ib}^T & M_{bb} + M_f \end{bmatrix} \begin{bmatrix} \bar{\phi}_i \\ \bar{\phi}_b \end{bmatrix} [\omega_f]^2 \tag{12}$$

The modes are normalized here to satisfy

$$[GM_f] = [\bar{\phi}]^T [M][\bar{\phi}] + [\bar{\phi}_b]^T [M_f][\bar{\phi}_b] = [I] \tag{13}$$

The basic assumption is that the structural displacements of the component in subsequent dynamic analysis can be expressed as a linear combination of n_f low-frequency modes in $[\bar{\phi}]$, namely,

$$\begin{Bmatrix} u_i \\ u_b \end{Bmatrix} = \begin{bmatrix} \bar{\phi}_i \\ \bar{\phi}_b \end{bmatrix} \{\xi_f\} \tag{14}$$

where $\{\xi_f\}$ is a vector of generalized displacements.

The fictitious masses cause local near-boundary deformations in the low-frequency modes. Previous FM applications[11,13,15] showed that the accuracy in subsequent analyses was not sensitive to the values in $[M_f]$ as long as the diagonal values were large enough to cause significant local deformations and not large enough to cause numerical ill-conditioning. Recommended values were of the order of the mass and moments of inertia of the entire component. Nevertheless, to present new applications and to gain more insight through comparisons with competitive methods, we deal first with the case of much larger fictitious masses.

Very Large Fictitious Masses

Very large masses in the context of this work are larger than those of the entire structural component by about six orders of magnitude. Such masses are sometimes used to analyze structural dynamic response to base accelerations[19] to eliminate the effects of inertial response forces on the accelerations of the large moving base. The use of even larger masses may cause numerical difficulties. In this section, we use very large masses to define a diagonal $[M_f]$, which loads the boundary coordinates instead of clamping them to the ground as in the fixed-boundary methods described earlier.

When the boundary is statically determined, the n_b lowest frequencies are zero and the associated modes are of rigid-body displacements. When the boundary coordinates are overdetermined, the first n_b frequencies are still almost zero because of the large masses, but the associated modes contain strain energy. The mode matrix $[\bar{\phi}]$ of Eqs. (12–14) is column-partitioned into the first n_b constraint modes, with subscript c, and the remaining modes with subscript n. At least one term in each column of the partition $[\bar{\phi}_{bc}]$ of the constraint modes is of the order of the maximal term in the associated column in $[\bar{\phi}_{ic}]$. Hence, it can be deduced that the effects of the original structural mass terms on the constraint-mode-generalized masses in Eq. (13) are negligible, which implies that

$$[\bar{\phi}_{bc}]^T [M_f][\bar{\phi}_{bc}] = [I] \tag{15}$$

which does not have a unique solution for $[\bar{\phi}_{bc}]$. A possible solution is

$$[\bar{\phi}_{bc}] = [M_f]^{-\frac{1}{2}} \tag{16}$$

This solution is enforced in MSC/NASTRAN[19] by assigning a SUPORT statement to the boundary coordinates. Equation (16) and the upper partition of Eq. (12), with the constraint modes and the associated zero frequencies, yield the static equilibrium equation

$$[K_{ii}][\bar{\phi}_{ic}] + [K_{ib}][M_f]^{-\frac{1}{2}} = [0] \tag{17}$$

which is solved for the interior displacements $[\bar{\phi}_{ic}]$ of the constraint modes. A comparison between Eqs. (4) and (17) shows that the CB constraint modes are related to the constraint modes in this section by

$$\begin{bmatrix} \phi_c \\ I \end{bmatrix} = \begin{bmatrix} \bar{\phi}_{ic} \\ \bar{\phi}_{bc} \end{bmatrix} [M_f]^{\frac{1}{2}} \tag{18}$$

The rest of the modes in Eq. (12), and the associated natural frequencies, are practically identical to the fixed-boundary vibration modes in Eqs. (2), (3), and (5), namely,

$$[\phi_n] = [\bar{\phi}_{in}] \tag{19}$$

However, the matrix of boundary displacements in these modes $[\bar{\phi}_{bn}]$ is not identically zero. The orthogonality in Eq. (13) between the constraint modes and the other modes, and Eqs. (18) and (19), yield

$$\left([\phi_c]^T[M_{ii}] + [M_{ib}]^T\right)[\phi_n] + \left([\phi_c]^T[M_{ib}] + [M_{bb}] + [M_f]\right)[\bar{\phi}_{bn}] = [0] \tag{20}$$

where the first term is equal to the mass-coupling matrix $[L]$ of Eq. (9). Since $[\phi_c]^T[M_{ib}]$ and $[M_{bb}]$ are negligible compared to $[M_f]$, $[L]$ can be calculated by

$$[L] = -[M_f][\bar{\phi}_{bn}] \tag{21}$$

where the small values in $[\bar{\phi}_{bn}]$ are multiplied by the large values in $[M_f]$.

To summarize this section, the data for CB modal coupling analysis, which is based on fixed-boundary modes, Eqs. (5) and (6), can be obtained by a single standard normal mode analysis, with the boundary coordinates loaded with very large masses. The first n_b resulting modes form the constraint modes $[\phi_c]$, whereas the remaining modes and natural frequencies are actually those of a fixed-boundary analysis $[\phi_n]$ and ω_n. The boundary displacements in the second mode group form the mass-coupling matrix $[L]$. When the boundary coordinates are statically determined, $[K_c] = [0]$ and $[M_c]$ is simply the rigid-body mass matrix. In overdetermined cases, the constraint modes are used to calculate $[M_c]$ and $[K_c]$ by Eqs. (7) and (8). To avoid numerical difficulties due to large factors between the actual and FM terms, it is recommended that the FM values be limited to about 10^6 times the respective inertial terms of the entire component.

Regular Fictitious Masses

Regular fictitious masses can be of the order of the mass of the entire component, or even larger, but still much smaller than the very large masses of the preceding section. We can no longer distinguish, in this case, between constraint modes and natural modes of the original structure. On the other hand, we can now treat the fictitious masses as regular mass terms without causing numerical difficulties.

The substitution of Eq. (14) in the original equation of motion (1) and premultiplication by $[\bar{\phi}]^T$ using Eq. (13) yield

$$\left([I] - [\bar{\phi}_b]^T[M_f][\bar{\phi}_b]\right)\{\ddot{\xi}_f\} + [\omega_f]^2\{\xi_f\} = [\bar{\phi}_b]^T\{F_b\} \tag{22}$$

where the fictitious masses are removed. The application of Eq. (22) with very large fictitious masses may cause numerical difficulties because it involves the multiplication of very large terms in $[M_f]$ by very small ones in $[\bar{\phi}_b]$.

The original formulation of the FM method[1,11] used Eq. (22) for modal coupling with other components. To facilitate easy implementation in standard finite element procedures for modal coupling and other applications and to gain more insight on the effects of the fictitious masses, the generalized coordinates are first transformed to those of the original free-boundary component. Equation (22) with zero right-hand side can be easily solved for all its n_f natural frequencies $[\omega_m]$ and eigenvectors $[\psi]$, which are normalized to unit-generalized masses,

$$[GM_m] \equiv [\psi]^T\left([I] - [\bar{\phi}_b]^T[M_f][\bar{\phi}_b]\right)[\psi] = [I] \tag{23}$$

The associated vibration modes in discrete coordinates are

$$\begin{bmatrix} \phi_i \\ \phi_b \end{bmatrix} = \begin{bmatrix} \bar{\phi}_i \\ \bar{\phi}_b \end{bmatrix} [\psi] \tag{24}$$

As will be demonstrated in the numerical application, the low frequencies in $[\omega_m]$ and the associated modes in $[\phi]$ are typically almost identical to those extracted from the unloaded finite element model. The high frequencies and modes reflect local deformations and are not necessarily actual natural modes.

To use the cleaned modes $[\phi]$ as generalized coordinates, the modal displacements of Eq. (22) are transformed by

$$\{\xi_f\} = [\psi]\{\xi_m\} \tag{25}$$

Given that $[\psi]$ is a square, nonsingular matrix, the transformation does not add errors beyond those introduced by the basic assumption of Eq. (14). The substitution of Eq. (25) in Eq. (22) and premultiplication by $[\psi]^T$ while using Eqs. (23) and (24) yield

$$\{\ddot{\xi}_m\} + [\omega_m]^2\{\xi_m\} = [\phi_b]^T\{F_b\} \tag{26}$$

which forms a standard modal representation of a structural component in dynamic analysis. The transformation implies, through Eqs. (14) and (24), that the discrete displacements of the component are recovered by

$$\begin{Bmatrix} u_i \\ u_b \end{Bmatrix} = \begin{bmatrix} \phi_i \\ \phi_b \end{bmatrix} \{\xi_m\} \tag{27}$$

The formulation of this section can be applied in modal coupling, as shown in the next section, or to other dynamic analyses such as response to local excitation at the boundary coordinates[15] or large structural changes near the boundary.[13,14] The method is efficient only when the masses are added at a relatively small number of coordinates. Moderately distributed excitation and structural changes[15,20] can be accurately considered with a fairly small number of modes without using fictitious masses. Modal structural damping coefficients may be added with a $\{\dot{\xi}_m\}$ term.

Free-Boundary Modal Coupling

A component (A), represented by the generalized model of Eq. (26), is connected to another component (B) through their boundary coordinates $\{u_b\}$. To perform this connection, each boundary coordinate must appear as an independent degree of freedom in at least one of the two components. In our case, $\{u_b\}$ is dependent in component A, Eq. (27), and independent in component B. One way to model component B is in its discrete coordinates; this method is used when component B is very simple or when it is changed frequently while component A remains unchanged. Another way is to model component B by the fixed-boundary modal representation of Eq. (6). This way is very convenient when a central structure is to be mounted with multiple payload configurations, as in Ref. 11, where the free-boundary modes of a fighter aircraft were coupled with fixed-boundary modes of various external stores. In this way, both components can be modeled by using fictitious masses, A with regular masses and B with very large ones.

To couple the fixed-boundary and free-boundary component modes, we take into account that, whereas $\{u_b\}$ of Eq. (6) and that of Eq. (27) are equal, $\{F_b\}$ of Eq. (6) and that of Eq. (26) are equal in size but have opposite signs. The substitution of $\{u_b\} = [\phi_b]\{\xi_m\}$ of Eq. (27) in Eq. (6), the premultiplication of the bottom row by $[\phi_b]^T$, and the substitution of $[\phi_b]^T\{F_b\}$ from Eq. (26) with reversed sign yield

$$\begin{bmatrix} I & L^T\phi_b \\ \phi_b^T L & I + \phi_b^T M_c \phi_b \end{bmatrix} \begin{Bmatrix} \ddot{\xi}_n \\ \ddot{\xi}_m \end{Bmatrix} + \begin{bmatrix} \omega_n^2 & 0 \\ 0 & \omega_m^2 + \phi_b^T K_c \phi_b \end{bmatrix} \begin{Bmatrix} \xi_n \\ \xi_m \end{Bmatrix} = \{0\} \tag{28}$$

which can be used for normal-mode analysis of the combined structure or for dynamic analyses where excitation and damping terms can be added.

The process that combines Eqs. (6) and (26) to obtain Eq. (28) is actually that of multipoint constraints (MPC) in standard finite element codes,[19] where $\{u_b\} = [\phi_b]\{\xi_m\}$ defines the constraints. The interior displacements for calculating generalized excitation forces and discrete response parameters are related to the generalized displacements by Eq. (27) for component A and by Eq. (5) for component B.

Component B can also be based on regular FM modes (of type A)[18] but only when n_b of its generalized coordinates are replaced by $\{u_b\}$. This replacement can be utilized in standard codes by applying $\{u_b\} = [\phi_b]\{\xi_m\}$ (of component B) as MPC statements with a subset $\{\xi_{m_1}\}$ of $\{\xi_m\}$ declared dependent (instead of $\{u_b\}$, provided the partition $[\phi_{b_1}]$ is not singular). The resulting model is similar in structure to that of Eq. (6), with the remaining $\{\xi_{m_2}\}$ of component B and $\{\xi_m\}$ of component A serving as generalized coordinates.

Design Loads

The dynamic response to external excitation is often used to define loading cases for structural design. The detailed structural design is based on static equilibrium between the internal elastic forces and a loading vector $\{F_s(t)\}$ at a selected time point t,

$$[K]\{u(t)\} = \{F_s(t)\} \tag{29}$$

The loading vector can be calculated from the modal response by either the summation-of-force (SOF) method that sums the external forces and the inertial and damping response forces, or the mode-displacement (MD) method that is based on the modal displacements only. The MD method is usually easier to apply but might be inaccurate. Reference 15 compared the two methods in cases of aeroelastic response to local impulsive excitation and showed that, with regular fictitious masses at the excitation points, the two methods are almost as accurate. With $\{u(t)\}$ of Eq. (29) approximated by Eq. (27), the MD loading vector becomes

$$\{F_s(t)\} = [K][\phi]\{\xi_m(t)\} \tag{30}$$

which, as deduced from Eqs. (12) and (24), can also be calculated by

$$\{F_s(t)\} = [K][\bar{\phi}]\{\xi_f(t)\} = [\bar{M}_f][\bar{\phi}][\omega_f]^2\{\xi_f(t)\} \tag{31}$$

where $[\bar{M}_f]$ is the mass matrix with the fictitious masses. Computations with the second expression are preferable because the mass matrix is usually much sparser than the stiffness matrix.

Detailed loading cases for stress analysis are calculated only at extreme conditions. The time points at which extreme conditions occur are defined by criticality criteria based on selected integrated loads, such as shear force and bending moments at a cross section. Section loads are calculated by integrating the distributed loads over the structure, between the section and a free end, with multiplication by the appropriate arms for section moments. A matrix $[\phi_l]$ of kinematic load modes is defined for the numerical integration. The load modes are used to produce MD section loads, for example, from the load case of Eq. (31) by

$$\{L_s(t)\} = [\phi_l]^T[\bar{M}_f][\bar{\phi}][\omega_f]^2\{\xi_f(t)\} \tag{32}$$

The shape of a load mode in $[\phi_l]$ is that of a broken structure with rigid-body segments. The definition of $[\phi_l]$ and the matrix operations to obtain the load coefficient matrices are not standard features of common finite element codes. A technique that simplifies the matrix operations and facilitates a convenient way to define load modes was applied by Karpel[20] for control surfaces and later extended[15] to overdetermined connections between the structural segments. The technique is reformulated here in a more general way that relates it to the other FM topics of this paper.

A structural section is defined here as a cut along element borders that divides the structure such that one part can move relative to the other one as a rigid body. The section grid points are duplicated and defined such that the outboard points are connected to the movable segment and the collocated inboard ones are connected to the remaining structure. A new grid point, whose n_l deflections $\{u_l\}$ represent the relative motion, is added at the section. The outboard displacements are related to the inboard ones and to $\{u_l\}$ by

$$\{u_o\} = \{u_i\} + [T_{rb}]\{u_l\} \tag{33}$$

which can be utilized in NASTRAN by MPC statements where $[T_{rb}]$ reflects a rigid-body transformation. The directions in $\{u_l\}$ that are not of interest can be constrained to zero. The remaining ones are loaded with very large fictitious masses in the diagonal $[M_l]$. A model can include several load sections simultaneously.

The new model has n_l more degrees of freedom than the original one. One can draw an analogy between the load modes and the constraint modes that were created earlier with very large masses. Normal-mode analysis produces two sets of modes with unit-generalized masses. The first n_l modes, $[\tilde{\phi}_l]$, appear as rigid-body modes, where the inboard segment does not move and the outboard one is kinematically defined by the relative motion. Similarly to Eqs. (18) and (19), the load modes are related to $[\tilde{\phi}_l]$ by $[\phi_l] = [\tilde{\phi}_l][M_l]^{1/2}$. The other modes $[\tilde{\phi}_f]$ are practically identical to the vibration modes without the section loads. Since the load modes and the structural modes are extracted in the same eigensolution, they are orthogonal, which yields, similarly to Eq. (20), a simple expression for the mass coupling between the vibration and the load modes,

$$[L_l] \equiv [\phi_l]^T[\bar{M}_f][\tilde{\phi}_f] = -[M_l][\tilde{\phi}_{fl}] \tag{34}$$

where $[\tilde{\phi}_{fl}]$ is the part of $[\tilde{\phi}_f]$ associated with $\{u_l\}$, which implies that the integrated MD loads can be easily computed by

$$\{L_s(t)\} = [L_l][\omega_f]^2\{\xi_f(t)\} \tag{35}$$

One can interpret the masses in $[M_l]$ as numeric load sensors that do not affect the structural dynamics.

Numerical Examples

Even though the previous applications of fictitious masses were based on different ad hoc formulations, they were still adequate demonstrations of the method's accuracy. The applications included wing-fuselage[1] and wing-stores[11] modal coupling, dynamic loads in response to store ejection,[15] stability of control-augmented structures,[12] and time simulation of an aeroelastic system with large local stiffness changes.[13,14]

The applications in this paper are given to compare the FM accuracy with CB models and to show the effects of the fictitious masses on the modal coordinates. The numerical examples are based on the 54-bay, 19-m, 74-kg truss shown in Fig. 1, which was constructed for ground tests of space structures.[18,21] Whereas the finite element model construction and normal-mode analyses were performed using MSC/NASTRAN, the reduced-size modal-coupling eigensolutions were performed using MATLAB. All the computations were performed with double-precision, 64-bit arithmetic.

A grid point was added at the middle of the near-end section, rigidly connected to the four section points, and loaded with very large masses of 10^8 in x, y, z, 10^6 in θ_x, and 10^{10} in θ_y and θ_z, which are about 10^6 larger than the rigid-body mass terms about this point (M_c in Table 1). For convenience, the mass units, kg in translation and kgm^2 in rotation, are omitted in what follows. The resulting 24 normal modes were used to construct the fixed-boundary CB model of Eq. (6), as explained after Eq. (21) for the case of a statically determined connection. The resulting elastic frequencies and the associated diagonal effective masses, Eq. (10), are given in Table 1. They are identical to those calculated directly for the clamped model.

The sum of the effective masses in Table 1 varies from 80% of the respective rigid-body masses in x to almost 100% in θ_y and θ_z. The

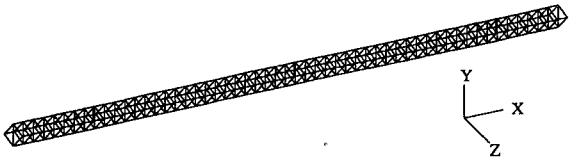

Fig. 1 Original truss.

Table 1 Natural frequencies, clamped end

No.	Freq., Hz	Mass, kg			Inertia, kgm^2		
		x	y	z	θ_x	θ_y	θ_z
1	0.19	0.00	45.1	0.00	0.00	0	8767
2	0.19	0.00	0.00	45.1	0.00	8765	0
3	1.18	0.00	13.9	0.00	0.02	0	224
4	1.19	0.00	0.00	13.9	0.00	226	0
5	3.26	0.00	4.78	0.00	0.02	0	27
6	3.27	0.01	0.00	4.84	0.00	29	0
7	3.73	0.00	0.03	0.00	3.69	0	3
8	6.27	0.00	2.46	0.00	0.00	0	7
9	6.27	0.18	0.00	2.50	0.00	8	0
10	9.25	57.7	0.00	0.03	0.00	0	0
11	10.1	0.00	1.48	0.00	0.01	0	3
12	10.1	1.49	0.00	1.50	0.00	3	0
13	11.2	0.00	0.02	0.00	0.40	0	0
14	14.7	0.03	0.00	1.04	0.00	1	0
15	14.7	0.00	1.01	0.00	0.00	0	1
16	18.7	0.00	0.00	0.00	0.15	0	0
17	19.8	0.01	0.00	0.75	0.00	0	0
18	19.9	0.00	0.73	0.00	0.00	0	0
	Total	59.4	69.6	69.6	4.30	9032	9033
	Diag. M_c	74.1	74.1	74.1	4.63	9033	9033

Table 2 Natural frequencies, free-free, $n_b = 3$

No.	Direct	FM	Error, %	CB	Error, %
1	1.191	1.191	0.00	1.191	0.00
2	3.243	3.244	0.02	3.244	0.02
3	6.244	6.247	0.06	6.248	0.06
4	10.081	10.091	0.10	10.093	0.12
5	14.645	14.666	0.14	14.673	0.18
6	18.363	19.547	6.45	19.781	7.72
7	19.825	20.046	1.11	20.972	5.78
8	25.491	58.902	120.04	60.287	136.50

effective masses indicate the level of coupling between motion in different directions. It can be observed that the lateral-axial motion in the x–z plane (modes 2, 4, 6, 9, 10, 12, 14, and 17, where only mode 10 is mainly axial) is totally uncoupled with the vertical-torsional motion. This is because the arrangement of the diagonal columns in the structure are such that x–z is a plane of symmetry and x–y is not. For simplicity and clarity, we deal here with the lateral-axial motion only, with three rigid-body modes.

A regular FM model was constructed by changing each of the very large mass terms at the end section to $m_f = 50$, which is still quite large compared to the actual mass of the end zone. The resulting model, Eq. (22), was used to calculate the free-free frequencies $[\omega_m]$, which are compared in Table 2 to those calculated directly from the finite element model. All the frequencies here are of lateral bending modes, except for mode 6, which is axial. The free-free frequencies, calculated from the CB model Eq. (6), with the right side equal to zero, also appear in Table 2. The accuracy of the first group of five frequencies in both cases is similar and very high. Since the number of boundary coordinates is three, the large errors in the last three frequencies were expected. The FM errors are slightly smaller. The variation of the FM frequency percentage errors with a uniform change in the m_f values from 1 to 10^6 is shown in Fig. 2. The error level increases with m_f, with moderate changes above $m_f = 50$, and approaches that of the CB model. The first-group errors at $m_f = 10^6$ are not shown. They are negative as a result of numerical difficulties in constructing and solving Eq. (22) with the very large $[M_f]$ and the very small $[\bar{\phi}_b]$.

The regular FM models were also used to calculate the clamped-end frequencies by replacing the three rigid-body modes by the three discrete boundary coordinates in $\{u_b\}$, as discussed after Eq. (28), and then setting $\{u_b\} = 0$. The percentage deviations of the eight resulting frequencies, from the nominal frequencies of Table 1, vs m_f are shown in Fig. 3. The largest error is that of the axial mode, which starts at 14% and drops below 1% at $m_f = 50$. All the other errors start at 4–8% and drop below 1% at $m_f = 10$. The effects of connecting the truss at its boundaries to other components would be somewhere between the free and clamped conditions. Table 2 and Figs. 2 and 3 indicate that the FM method is robust to the choice of fictitious masses, provided they are relatively large but not large enough to cause numerical difficulties.

Table 3 Natural frequencies, free-free, $n_b = 5$

No.	Direct	FM	Error, %	CB	Error, %
1	1.191	1.191	0.01	1.191	0.01
2	3.243	3.245	0.05	3.245	0.06
3	6.244	6.256	0.19	6.259	0.24
4	10.081	10.121	0.39	10.131	0.50
5	14.645	14.978	2.27	15.079	2.97
6	18.363	19.596	6.71	20.323	10.68
7	19.825	20.473	3.27	21.123	6.54
8	25.491	27.142	6.47	27.738	8.82
9	31.566	76.211	141.44	82.281	160.67

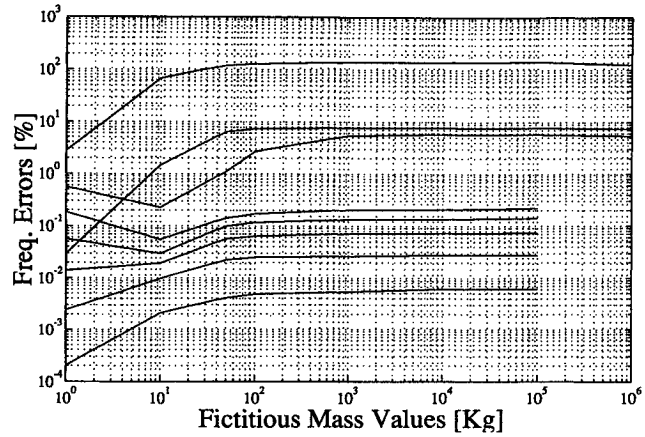

Fig. 2 Free-free frequency errors vs m_f.

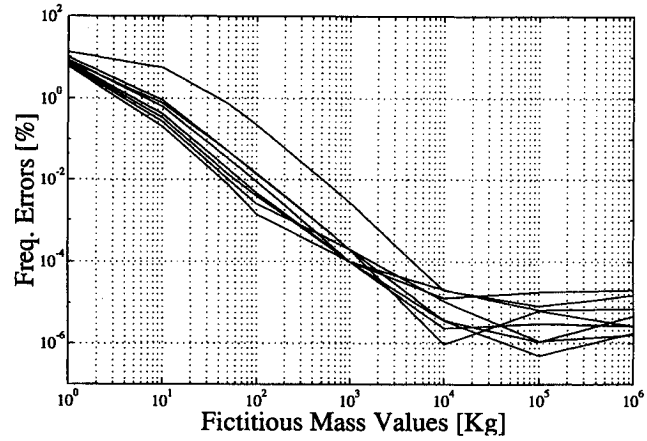

Fig. 3 Clamped frequency errors vs m_f.

To demonstrate the FM and CB models in cases of overdetermined boundary, two boundaries coordinated in z, one after bay 18 and one after bay 40, were added to the three end coordinates. The FM model was constructed with all the boundary masses equal to 50. Twelve coordinates were considered in both models, Eq. (6) for the CB model and Eq. (26) for the FM one. The nine free-boundary elastic frequencies obtained from the two models are compared with the direct ones in Table 3, where all the modes are lateral except for 6, which is axial. The number of modes in the high-error group is now 5. As in the $n_b = 3$ case, the errors in the first group are very low, and the FM errors are lower than the CB ones, especially in the second group.

The lateral FM modes of Table 3 (all except the axial mode 6) are compared with the respective direct modes in Fig. 4. It can be observed that the FM and direct modes in the low-error group are practically identical. The first two FM modes in the high-error group are also very close to the direct ones. The local deformations

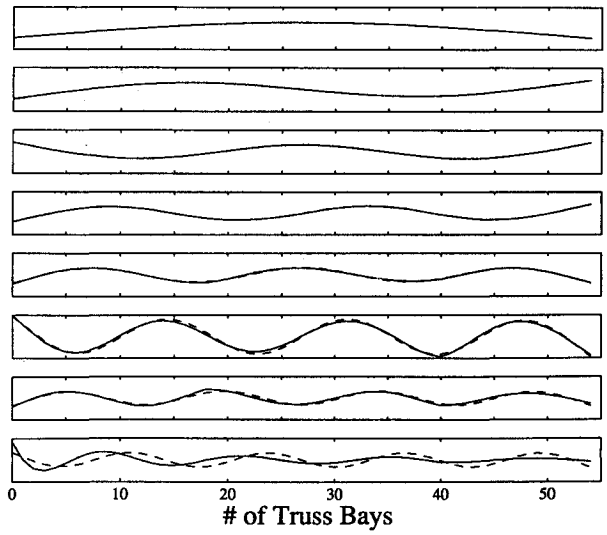

Fig. 4 Lateral mode shapes, free-free, n_b = 5: ——, FM and ----, direct.

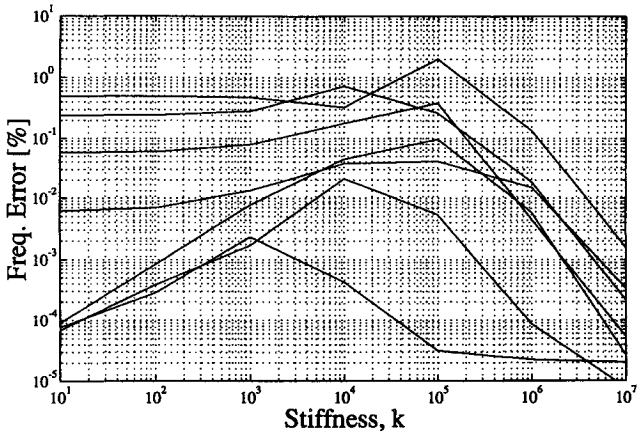

Fig. 5 CB frequency errors, clamped through springs.

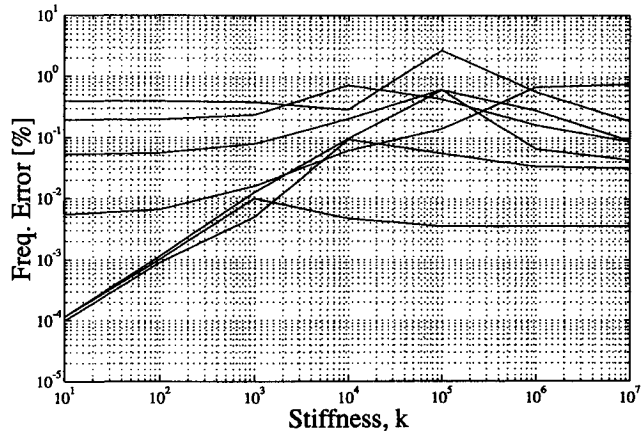

Fig. 6 FM frequency errors, clamped through springs.

at the near end (at 0) and after bays 18 and 20 are significant in the last two modes. These deformations are essential for high-accuracy accounting of the effects of forces applied by neighboring structural components or by other external excitations.

To show these models as part of larger structures without getting too complicated, the models were connected to the ground using five springs of equal value. Computations were repeated for the direct, FM, and CB models, with k varying from 10 to 10^7 (N/m in translation and Nm/rad in rotation). The percentage errors of the seven lowest frequencies, relative to the sequentially respective direct frequencies, are shown vs k in Fig. 5 for CB and Fig. 6 for

Table 4 Natural frequencies of the assembled structure, n_b = 5

No.	Direct	Coupling	Error, %
1	0.279	0.279	0.00
2	1.330	1.330	0.00
3	2.628	2.628	0.01
4	4.828	4.828	0.00
5	6.165	6.166	0.01
6	8.659	8.659	0.00
7	9.092	9.093	0.02
8	10.739	10.745	0.05
9	12.831	12.835	0.03
10	15.264	15.267	0.02
11	16.832	16.847	0.08
12	21.355	21.374	0.09
13	23.459	23.522	0.27
14	27.801	27.808	0.02
15	28.408	28.425	0.06
16	32.187	32.315	0.40
17	35.945	36.105	0.45
18	39.135	39.137	0.01
19	45.256	45.877	1.37
20	45.598	46.570	2.13
21	46.494	47.040	1.17
22	57.700	57.741	0.07
23	59.231	60.028	1.34
24	59.512	62.240	4.58
25	64.939	186.90	187.81
26	65.622	671.71	923.60
27	73.273	392.95	5262.9

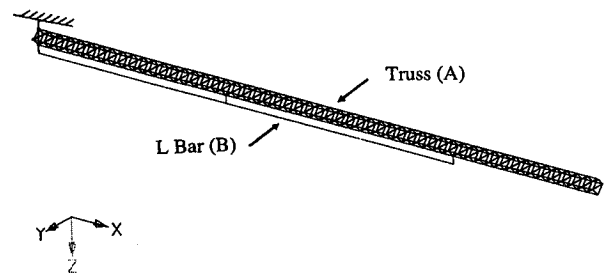

Fig. 7 Combined truss-bar model.

FM. The accuracy levels are similar in almost the entire range, except at high k values, where the springs are practically rigid, as in the basic CB model. It is obvious that the FM method would be more accurate when masses are added instead of springs.

The last demonstration of the use of the FM method is a typical substructure synthesis with two dissimilar components. In this example, we wish to accurately obtain the frequencies of the system shown in Fig. 7, which combines the truss model used in the previous examples (component A) with a clamped L-shaped bar (component B). The two components are interconnected through the five boundary coordinates of the previous example. The frequency range of interest for the coupled system is 0–30 Hz. To yield good accuracy in this range, the modes describing each component should cover approximately twice this range, namely, 0–60 Hz.

Component A is represented by a 20-mode FM model of Eq. (26). To construct this model, the five boundary coordinates of the finite element truss model were loaded with FM terms of 100 kg in translation and 100 kgm^2 in rotation. It is clear that the size of the fictitious masses is significantly larger than actual mass terms of the 74-kg truss but not too large. The lowest 20 frequencies, ranging from 0 to 59 Hz, and the associated modes of the mass-loaded truss were used to obtain the FM model of the free, unloaded truss, according to Eqs. (22–24). The resulting free-truss frequencies used in Eq. (26) lie between 0 and 173 Hz.

Component B is a 175-kg beam-type structure modeled by 46 bar elements. It is represented in the modal coupling by the CB model of Eq. (6) with five constraint modes and seven clamped vibration modes. The 12 modes were obtained by loading the boundary coordinates with very large masses of 10^8 kg in translation and 10^{10} kgm^2

in rotation, defining them as SUPORT coordinates, and performing a regular normal-mode analysis. The resulting modes, between 4.7 and 61 Hz, were used to define the CB modes by Eqs. (18) and (19). The two models were combined according to Eq. (28), which was used to obtain the 27 eigenvalues of the coupled system. The coupling frequencies are compared in Table 4 to those calculated directly for the combined finite element system. It can be observed that the first 15 frequencies, those in the frequency range of interest, are practically in perfect agreement with the direct frequencies.

Conclusions

The FM method was formulated in a general way that is applicable to various modal-based problems with important local effects. Being based on a single set of modes calculated by a standard normal-mode analysis, it can be easily integrated in standard finite element codes. The accuracy of the coupling models obtained by the FM method is similar to that of the CB method in the low-frequency range and is somewhat better in the high-frequency range. The FM method includes free-boundary normal modes as generalized coordinates, and it does not require the interface coordinates to be retained in the model as the CB method does. A disadvantage of the FM method is that it requires the selection of the fictitious mass values. This is not a significant disadvantage, however, because the method is very robust to the values of the fictitious masses in a very wide and easily defined range. A version of the FM method for very large boundary masses forms easy ways to obtain CB models, effective masses, and load modes for dynamic loads analyses. The described procedures allow the simultaneous assignment of fictitious masses for different purposes.

References

[1]Karpel, M., and Newman, M., "Accelerated Convergence for Vibration Modes Using the Substructure Coupling Method and Fictitious Coupling Masses," *Israel Journal of Technology*, Vol. 13, May 1975, pp. 55–62.

[2]Hurty, W. C., "Dynamic Analysis of Structural Systems by Component Modes," *AIAA Journal*, Vol. 3, No. 4, 1965, pp. 678–685.

[3]Craig, R. R., Jr., and Bampton, M. C. C., "Coupling of Substructures for Dynamic Analyses," *AIAA Journal*, Vol. 6, No. 7, 1968, pp. 1313–1319.

[4]Girard, A., "Modal Effective Mass Models in Structural Dynamics," *Proceedings of the 9th International Modal Analysis Conference*, Society for Experimental Mechanics, Bethel, CT, 1991, pp. 45–50.

[5]Goldman, R. L., "Vibration Analysis by Dynamic Partitioning," *AIAA Journal*, Vol. 7, No. 6, 1969, pp. 1152–1154.

[6]Hou, S. N., "Review of Modal Synthesis Techniques and a New Approach," *Shock and Vibration Bulletin*, Vol. 40, Pt. 4, 1969, pp. 25–30.

[7]Benfield, W. A., and Hruda, R. F., "Vibration Analysis of Structures by Component Mode Substitution," *AIAA Journal*, Vol. 9, No. 7, 1971, pp. 1255–1261.

[8]Hintz, R. M., "Analytical Methods in Component Modal Synthesis," *AIAA Journal*, Vol. 13, No. 8, 1975, pp. 1007–1016.

[9]Rubin, S., "Improved Component-Mode Representation in Structural Dynamic Analysis," *AIAA Journal*, Vol. 13, No. 8, 1975, pp. 995–1006.

[10]Tran, D. M., "Hybrid Methods of Component Mode Synthesis," *Proceedings of the International Forum on Aeroelasticity and Structural Dynamics*, Vol. 2, Association Aeronautique et Astronautique de France, Paris, France, 1993, pp. 911–925.

[11]Karpel, M., "Efficient Vibration Mode Analysis of Aircraft with Multiple External Store Configurations," *Journal of Aircraft*, Vol. 25, No. 8, 1988, pp. 747–751.

[12]Livne, E., "Accurate Calculation of Control Augmented Structural Eigenvalue Sensitivities Using Reduced Order Models," *AIAA Journal*, Vol. 27, No. 7, 1989, pp. 947–954.

[13]Karpel, M., and Wieseman, C. D., "Modal Coordinates for Aeroelastic Analysis with Large Local Structural Variations," *Journal of Aircraft*, Vol. 31, No. 2, 1994, pp. 396–403.

[14]Karpel, M., and Wieseman, C. D., "Time Simulation of Flutter with Large Stiffness Changes," *Journal of Aircraft*, Vol. 31, No. 2, 1994, pp. 404–410.

[15]Karpel, M., and Presente, E., "Structural Dynamic Loads in Response to Impulsive Excitation," *Journal of Aircraft*, Vol. 32, No. 4, 1995, pp. 853–861.

[16]Gwinn, K. W., Lauffer, J. P., and Miller, A. K., "Component Mode Synthesis Using Experimental Modes Enhanced by Mass Loading," *Proceedings of the 6th International Modal Analysis Conference*, Society for Experimental Mechanics, Bethel, CT, 1988, pp. 1088–1093.

[17]Admire, J. R., Tinker, M. L., and Ivey, E. W., "Mass-Additive Modal Test Method for Verification of Constrained Structural Models," *AIAA Journal*, Vol. 31, No. 11, 1993, pp. 2148–2153.

[18]Karpel, M., Raveh, D., and Ricci, S., "Ground Vibration Tests of Space-Structure Components Using Boundary Masses," 45th Congress of the International Astronautical Federation, Jerusalem, Israel, Oct. 1994 (IAF Paper 94-I.2.185).

[19]Blakely, K., "MSC/NASTRAN Basic Dynamic Analysis," User's Guide, V68, MacNeal–Schwendler Corp., Los Angeles, CA, 1993.

[20]Karpel, M., "Multidisciplinary Optimization of Aeroservoelastic Systems Using Reduced-Size Models," *Journal of Aircraft*, Vol. 29, No. 5, 1992, pp. 939–946.

[21]Bernelli Zazzera, F., Gallieni, D., and Ricci, S., "Modal Testing of a Large Space Structure Laboratory Model," *Proceedings of the 17th International Seminar on Modal Testing*, Vol. 2, Katholike Universiteit Lueven, Lueven, Belgium, 1992, pp. 1177–1190.